ISCI, Volume *22*

Supplemental Information

Utilizing Polymer Micelle to Control Dye J-aggregation and Enhance Its Theranostic Capability

Chen Shao, Fan Xiao, Heng Guo, Jiantao Yu, Dong Jin, Changfeng Wu, Lei Xi, and Leilei Tian

TRANSPARENT METHODS

Chemicals and materials. Chemicals and solvents were used as received without further purification, unless specified otherwise. DNA sequences (HPLC purified), thiazolyl blue tetrazolium bromide (MTT), calcein acetoxymethyl ester (Calcein-AM), propidium iodide (PI), and tubular dialyzer (50,000-molecular-weight cutoff, 2.5 mL) were obtained from Sangon Biotech Co., Ltd. (Shanghai, China). Indocyanine green (ICG) was purchased from TCI Chemical Industry Co., Ltd. (Japan). DSPE-PEG_{2k}-NH_2 was purchased from Shanghai Ponsure Biotech, Inc. (Shanghai, China). Acetic acid (HAc), sodium acetate (NaAc), doxorubicin hydrochloride (DOX), 4-Morpholineethanesulfonic acid (MES), 1-(3-(dimethylamino) propyl)-3-ethylcarbodiimide hydrochloride (EDC), N-hydroxysulfosuccinimide (NHS), and dimethyl sulfoxide (DMSO) were obtained from Aladdin Chemistry Co., Ltd. (Shanghai, China). The acetic acid and N, N-diethylethanamine for preparing triethylammonium acetate buffer (TEAA), and the acetonitrile used in HPLC analysis were of HPLC grade and purchased from Energy Chemical Co., Ltd. (Shanghai, China). Doxil was obtained from the Shenzhen Second People's Hospital. Phosphate buffered saline (PBS) was prepared by dissolving tablets obtained from Amresco (Solon, OH, USA) in ultrapure water according to the manufacturer's instructions (10.0 mM PBS, containing 137.0 mM Na^+ and 2.0 mM K^+). Acetyl acetate solution (3.0%) and copper grid were purchased from Zhongjingkeyi Technology Co., Ltd. (Beijing, China). Ultrapure water (at 18.2 MOhm) was produced by a Millipore synergy UV Ultrapure water purification system (MA, USA). The ultrafiltration tube (100,000-molecular-weight cutoff, 15.0 mL) was also purchased from the Millipore Co. Ltd. A549 cells were kindly provided by Professor Ying Sun at the Department of Biology of Southern University of Science and Technology (SUSTech); L02 cells were purchased from Jennio Biotech Co., Ltd. (Guangzhou, China). RPMI 1640 medium, Dulbecco's modified

Eagle's medium (DMEM), trypsin-EDTA solution, fetal bovine serum (FBS), and penicillin/streptomycin were purchased from Gibco BRL Co., Ltd. (Grand Island, NY, USA). Male BALB/c nude mice and SD rats were purchased from Vital River Laboratory Animal Technology Co., Ltd. (Beijing, China).

Instruments. The 808- and 880-nm continuous-wave laser systems were purchased from Changchun Laser Technology Co., Ltd. (Changchun, China). The output power of the lasers was measured with a VLP-2000 laser power meter (Xi'an Hirsh Laser Tech. Co., Ltd., China). The transmission electron microscopy (TEM) images were carried out on Hitachi HT7700 (Hitachi, Japan); the samples were negatively stained with acetyl acetate and imaged by TEM. Specifically, a sample (5.0 μL) was dropped on the surface of a freshly plasma treated copper grid and kept for 2 min, and then the grid was blotted from the edge with a piece of filter paper; thereafter, 5.0 μL of acetyl acetate (1%) was dropped on the sample and kept for 2 min, and again the grid was blotted from the edge with a piece of filter paper to remove the excess acetyl acetate. The grids were completely dried in a vacuum oven prior to the test. The hydrodynamic diameters and zeta potentials of the micelles were determined by a NanoBrook ZetaPALS potential analyzer (Brookhaven Instruments Corporation, USA) in ultrapure water. The absorption calibration curve of ICG and the related absorption analysis, as well as the fluorescence calibration curves of DOX and Cy3-AS1411-COOH and the related fluorescence analysis were carried out on a Cytation 3 microplate reader (BioTek Instruments, Inc., Winooski, USA). The fluorescence spectra were taken by an iHR320 imaging spectrometer (Horiba, Japan). The ^{1}H NMR spectra were recorded on a Bruker Advance 400 instrument in D_2O using the residual signal from H_2O (^{1}H, $\delta = 4.79$ ppm) as the internal standard. The fluorescence images of cells were taken by a Leica TCS-SP8 laser scanning confocal microscope (LSCM, Leica, Germany) with excitation wavelengthes of 488 nm

(for Calcein-AM) and 561 nm (for PI). The *in vivo* fluorescence images were obtained by an IVIS Spectrum Imaging System (PerkinElmer, USA), with an excitation wavelength at 745 nm and the emission wavelength at 850 nm. In the photoacoustic imaging (PAI) experiments, a pulsed OPO laser (Surelite OPO, Continuum, CA, USA) pumped by a Q-switched Nd: YAG laser (Surelite I-20, Continuum, CA, USA) with a duration of 20 ns and a repetition rate of 20 Hz served as the photoacoustic excitation source. The laser beam was split and coupled into two optical fiber bundles. Induced photoacoustic waves were collected by a point-focused 7.5-MHz ultrasound transducer with 0.5-inch aperture and 1.0-inch focal length. The imaging interface consisting of transducer and optical fiber bundles was mounted on a two-dimensional (2D) moving stage that scanned two-dimensionally. The interval step was 0.1 mm in the scanning processes. The quantification analysis was performed by drawing the region of interests (ROIs) over the sample on the PAI images, and then measured the PAI signal intensity using Matlab (MathWorks Inc., MA, USA). The IR thermographic images were taken by a near infrared thermal imager (FLIR-E64501, FLIR Systems Inc., USA). An ACQUITY HPLC system (Waters Corporation, MA, USA) was employed for ICG-quantitation in the bio-distribution measurement. The blood routine test was conducted on a HF-3800 automated hematology analyzer (Healife, China) according to the operating instruction. The H&E stained tissue slices were examined by an Eclipse Ti-S optical microscope (Nikon, Japan).

Fabrication of DSPE-PEG@ICG-J. In a typical process, ICG (50 $\mu g \cdot mL^{-1}$) and DSPE-PEG_{2k}-HN_2 (0.1 $mg \cdot mL^{-1}$) were co-dissolved in ultrapure water; the mixture was heated at 80 ℃ for 15 min with vigorous stirring, and then stirred at room temperature for 8 h. The product was concentrated by ultrafiltration and stored at -4 ℃ for further use.

Fabrication of DSPE-PEG-1411@ICG-J/DOX. In a typical process, 1.0 mL of DSPE-PEG@ICG-J solution (1.5 $mg \cdot mL^{-1}$), 0.3 mL of EDC solution (1.5 M), 0.3 mL of NHS solution (1.5 M), and 50 μL of AS1411-COOH solution (200 μM) were mixed in 2.5 mL of MES buffer (0.5 M, pH 6.75) that containing 2.0 M of NaCl. The mixture was stirred at room temperature for 3 h, and ultra-filtrated to remove the small molecules and unreacted AS1411 aptamer, thus affording DSPE-PEG-1411@ICG-J. To fabricate DSPE-PEG-1411@ICG-J/DOX, 0.2 mL of DOX solution (4.0 $mg \cdot mL^{-1}$) and 0.5 mL of DSPE-PEG-1411@ICG-J solution (1.5 $mg \cdot mL^{-1}$) was mixed and shaken at 37 ℃ for 12 h. The product was purified by ultrafiltration and stored at -4 ℃ for further use.

Determination of the grafting efficiency of AS1411 aptamer and DOX loading efficiency on DSPE-PEG-1411@ICG-J/DOX. The grafting efficiency of AS1411 aptamer was quantitatively analyzed by fluorescence spectrophotometry. Therefore, Cy3-labelled aptamer sequence, Cy3-AS1411-COOH, was used to replace AS1411-COOH to proceed the graft reaction. The unreacted DNA sequences in the filtrate were collected after the ultrafiltration, whose fluorescence was measured and amount was quantified according to the fluorescence calibration curve of Cy3-AS1411-COOH (λ_{em} = 500 nm and λ_{ex} = 565 nm) (Figure S18A). Finally, the unreacted DNA amount was subtracted from the total amount of DNA in the reaction to calculate the DNA grafting amount. The final result was the average of three independent measurements.

The DOX loading efficiency was also determined by fluorescence spectrophotometry. The amount of unloaded DOX in the filtrate was quantified by the fluorescence calibration curve of DOX (λ_{em} = 595 nm and λ_{ex} = 488 nm) (Figure S18B), which was subtracted from the total amount of DOX to calculate the DOX loading amount on DSPE-PEG-1411@ICG-J. The final result was the average of three independent measurements.

The DNA sequences used in this work (from 5′ to 3′). AS1411-COOH: HOOC-3[$(CH_2$-$CH_2O)_6$]-GGT GGT GGT GGT TGT GGT GGT GGT GG. Cy3-AS1411-COOH: HOOC-3[$(CH_2$-$CH_2O)_6$]-GGT GGT GGT GGT TGT GGT GGT GGT GG-Cy3.

***In vitro* DOX release profile from DSPE-PEG-1411@ICG-J/DOX.** Two identical solutions of DSPE-PEG-1411@ICG-J/DOX (1.0 mL each, ICG concentration equivalent to 150.0 μg·mL^{-1}) were dialyzed against PBS buffer (10.0 mL, 10.0 mM, pH 7.4) and HAc-NaAc buffer (10.0 mL, 10.0 mM, pH 5.5) at 37 ℃, respectively. At appropriate time points, the old dialysis buffers were replaced by the new one, and the old buffers were collected and the released DOX was quantified according to the fluorescence calibration curve of DOX (λ_{em} = 595 nm and λ_{ex} = 488 nm) (Figure S18B and S18C). The detection continued for 72 h, and the cumulative DOX release at a certain time point can be determined by the following equation:

$$A_T = \frac{\sum_{i=1}^{T} C_i \times 0.01(\mathrm{L})}{90.0\ \mu\mathrm{g}} \times 100\ \%$$

Where A_T stands for the cumulative DOX release at a certain time point; T stands for certain time point; C_i stands for the DOX concentration in the dialysis buffer which was collected at different time points (μg·L^{-1}); 90.0 μg was the total amount of DOX loaded on DSPE-PEG-1411@ICG-J/DOX.

Photothermal conversion efficiency and photostability determination. To determine the photothermal conversion efficiency, in a cuvette an aqueous solution of a sample (1.0 mL) with a certain ICG concentration was continuously irradiated for 500 s with an 880-nm laser at a power of 0.8 W·cm^{-2} (1 cm beam diameter), and the temperature was recorded every 10 s by a digital thermometer. Notably the sample of free ICG (50.0 μg·mL^{-1}) was irradiated with an 808-nm laser

(0.8 $W \cdot cm^{-2}$) according to its optimal absorption. Samples of pure water under the irradiation of 808- and 880-nm laser (0.8 $W \cdot cm^{-2}$) were detected as controls.

For photostability study, the temperatures of the aqueous solutions of various samples (ICG concentration equivalent to 50.0 $\mu g \cdot mL^{-1}$) were recorded every 10 s during five circles of 10-min with irradiation (heating) and 20-min without irradiation (cooling) processes, where the complex micelles based on ICG J-aggregate and free ICG were irradiated by 880- and 808-nm laser (0.8 $W \cdot cm^{-2}$), respectively, according to their maximal absorptions. The absorption spectra and photos of the solutions of free ICG and DSPE-PEG@ICG-J before and after the first test circle were recorded.

Cell culture. A549 and L02 cells were respectively maintained as monolayer cultures in DMEM and PRMI 1640 medium at 37 ℃ in an INCO2/153 CO_2 incubator (Memmert, Germany; 5% CO_2), both of the mediums were supplemented with 10% FBS and 1% penicillin/streptomycin. The cells were cultured until confluence was reached before each experiment.

Animal model. All animal experiments were in accord with Institutional Animal Use and Care Regulations, according to protocol No. SUSTC-JY2017078, approved by the Laboratory Animal Ethics Committee of the Southern University of Science and Technology. After being acclimated and tested for infectious diseases for 1 week, 4-week-old BALB/c nude mice were subcutaneously injected with A549 cells (1×10^7 cells each mouse) at the flank region. After about two weeks, mice with tumor volumes of about 80-150 mm^3 were randomized into treatment groups. The tumor size was calculated using the following formula: Volume = (Length $\times$ $Width^2$)/2.

***In vitro* and *in vivo* biostability determination.** First, 10% FBS was utilized to mimic the biological environment. Samples were dispersed in 10% FBS to form suspensions with ICG

concentrations equivalent to 10.0 μg·mL^{-1}, which were shaken at 37 ℃ for 24 h; the absorption spectra of the final samples were detected. To determine the biostability for intracellular application, samples were dispersed in basic DMEM to form suspensions with ICG concentrations equivalent to 10.0 μg·mL^{-1}, which were incubated with A549 cells (in the logarithmic growth phase) for 12 h at 37 ℃, thereafter, the cells were washed three times with PBS buffer, further digested with 0.25% (w/v) trypsin-0.03% (w/v) EDTA solution; The collected cells were centrifuged and re-suspended in PBS buffer (0.5 mL) for absorption spectra test. For *in vivo* biostability determination, samples (150.0 μL) with ICG concentrations equivalent to 0.5 mg·mL^{-1} were intravenously injected to BALB/c nude mice, and then the *in vivo* fluorescence images were obtained at different time points after the injection *via* the animal fluorescence imaging system.

Cellular uptake study. Free ICG, DSPE-PEG@ICG-J, DSPE-PEG-1411@ICG-J and DSPE-PEG-1411@ICG-J/DOX were dispersed in the basic DMEM (ICG concentration equivalent to 25.0 μg·mL^{-1}) and incubated with A549 cells in 6-well plates for 4 h at 37 ℃, the un-internalized samples were removed, thereafter, the cells were washed three times with PBS buffer, further digested with 0.25% (w/v) trypsin-0.03% (w/v) EDTA solution; The collected cells were centrifuged, and re-suspended in PBS buffer (1.0 mL) for cell counting. Next, the cells were centrifuged again and re-suspended in a mixed solvent of DMSO and H_2O (v/v = 4/1, and 1.0 mL total volume), and disrupted by an ultrasonic cell disruptor. Due to the presence of DMSO and the ultrasonic treatment, the micelles disassembled and ICG J-aggregates broke up to free ICG. Therefore, the cellular uptake amount of ICG was evaluated by the absorption calibration curve of free ICG (Figure S18D).

Cytotoxicity and *in vitro* anti-cancer therapy. To detect the dark cytotoxicity, A549 and L02 cells were seeded in 96-well plates and pre-cultured for 24 h, and then the mediums were replaced

by 90.0 μL of fresh medium along with 10.0 μL of sample suspension in PBS buffer with ICG concentrations equivalent to 0.0, 5.0, 10.0, 25.0, 50.0, 75.0 and 100.0 $\mu g \cdot mL^{-1}$. After a 4-h incubation, the cells were gently washed by PBS buffer for three times to remove the non-internalized samples, thereafter, the cells were cultured for another 24 h (37 ℃, 5% CO_2). The cell viabilities were determined by MTT assay, and the results were presented as average ± SD (n = 5).

For *in vitro* anti-cancer therapy study, A549 cells were seeded in 96-well plates and pre-cultured for 24 h, and then the mediums were replaced by 90.0 μL of fresh mediums along with 10.0 μL of sample suspension in PBS buffer with ICG concentrations equivalent to 0.0, 5.0, 10.0, 25.0, 50.0, 75.0 and 100.0 $\mu g \cdot mL^{-1}$. After 4-h incubation, the cells were gently washed by PBS buffer for three times to remove the non-internalized samples; Next, the cells were applied to laser irradiation (0.8 $W \cdot cm^{-2}$) for 10 min (Notably, 808 nm-laser for ICG and 880-nm laser for the micelle samples based on ICG J-aggregate), and then the cells were further cultured for 24 h (37 ℃, 5% CO_2). Finally, the cell viabilities were determined by MTT assay, and the results were presented as average ± SD (n = 5).

***In vitro* and *in vivo* photoacoustic imaging.** For in vitro photoacoustic tests, a cuboid container was filled with 2.0% agarose gel to half depth. Aqueous solutions of various samples (with different ICG equivalent concentrations ranging from 20.0 to 100.0 $\mu g \cdot mL^{-1}$) were filled into polyethylene capillaries, consequently, which were laid on the surface of the solidified agarose gel and further covered with thin 2.0% agarose gel to make the surface smooth.

For *in vivo* photoacoustic imaging, the aqueous solutions (150.0 μL) of various samples with an ICG concentration equivalent to 0.5 $mg \cdot mL^{-1}$ were intravenously injected to the mice. The PAI images were collected at different time points after the injection.

Blood circulation analysis and bio-distribution measurement. For the blood circulation analysis, three SD rats were administered with DSPE-PEG-1411@ICG-J/DOX at an ICG equivalent dose of 4 mg kg^{-1}. After predetermined time intervals (15 and 30 min; 1, 2, 4, 8, 12, 24, and 48 h), blood was taken from tail artery of SD rats and stored in heparinized tubes. To each blood sample (50 μL), 200 μL DMSO was added to convert the ICG J-aggregates in DSPE-PEG-1411@ICG-J/DOX to free ICG. The amount of ICG were measured by HPLC along with the absorption calibration curve of ICG (Figure S18E), and normalized to percentages of injected dose per gram of blood (% ID g^{-1}). A first order exponential decay was fitted to the data, giving an accurate model of the DSPE-PEG-1411@ICG-J/DOX blood clearance time. For the bio-distribution measurement, sample suspensions (150.0 μL) with an ICG concentration equivalent to 0.5 mg·mL^{-1} were injected into the A549 tumor-bearing mice *via* the tail vein. The mice were sacrificed 12 h after the injection (n = 3 for each group), and their tumors, livers, spleens, kidneys, lungs, and hearts were excised. All these tissues were weighed and homogenized in a cooled glass tissue grinder, and then ICG was extracted from the tissue slurries using a mixed solvent of DMSO and H_2O (v/v = 4/1)**.** Finally, the amount of ICG were measured by HPLC along with the absorption calibration curve of ICG (Figure S18E), and normalized to percentages of injected dose per gram of tissue (% ID g^{-1}).

HPLC quantification method: Flow rates were 0.5 mL·min^{-1}. Injection volumes were 50.0 μL. The column temperature was maintained at 40 ℃ throughout the analysis. UV absorbance was monitored at 780 nm. The gradient solvent system was TEAA (100.0 mM, pH 7.0)/acetonitrile. The percentage of acetonitrile linearly increased from 5% to 100% within the 20 min analysis period.

***In vivo* anticancer therapy.** The A549 tumor-bearing mice were randomly divided into 9 groups consisting of 4 mice in each group. The untreated mice in group i was used as a control. 150.0 μL of DOX in PBS buffer (0.3 $mg \cdot mL^{-1}$), PBS buffer, free ICG in PBS buffer (0.5 $mg \cdot mL^{-1}$) were injected sequentially to the mice *via* the tail vein, which were denoted as group ii to iv; 150.0 μL of DSPE-PEG@ICG-J and DSPE-PEG-1411@ICG-J in PBS buffer (ICG concentration equivalent to 0.5 $mg \cdot mL^{-1}$) were injected sequentially to the mice *via* the tail vein, respectively, which were denoted as group vii and viii. For the mice in both group vi and ix, 150.0 μL of DSPE-PEG-1411@ICG-J/DOX (ICG concentration equivalent to 0.5 $mg \cdot mL^{-1}$) were intravenously injected. 1 h after the injection, the mice in group iv were irradiated at their tumor sites by a 808-nm laser for 10 min (0.8 $W \cdot cm^{-2}$); 12 h after the injection, the mice in group iii, vii, viii, and ix were irradiated at their tumor sites by a 880-nm laser for 10 min (0.8 $W \cdot cm^{-2}$); no irradiation was applied to the mice in group i, ii, and vi. 12 h after the treatments, one mouse in each group was sacrificed by cervical dislocation for necropsy, and its tumor was collected for tissue slicing and staining. For the left mice, their tumor sizes were measured by utilizing a caliper every 2 days for a period of 24 days, and the tumor volumes were calculated using the following formula: Volume = $(\text{Length} \times \text{Width}^2)/2$. After the 24-day treatment, the mice in group ix were sacrificed by cervical dislocation for necropsy, their major organs including hearts, livers, spleens, lungs, and kidneys were harvested for tissue slicing and staining. For the mice in group v, 150.0 μL of Doxil in PBS buffer (DOX concentration equivalent to 0.3 $mg \cdot mL^{-1}$) was intravenously injected every 4 days for 3 times in total, and the day for conducting the first injection was designated as day 1. 12 h after the first treatment, one mouse was sacrificed by cervical dislocation for necropsy, and its tumor was collected for tissue slicing and staining. For the left mice, the tumor size measurement and tumor volume calculation were conducted according to the same method of other groups.

H&E staining. The tissues were fixed in 10 % neutral buffered formalin, processed routinely into paraffin, sectioned at 4 μm, stained with hematoxylin-eosin (H&E) and examined by optical microscope.

SUPPLEMENTAL TABLE

Table S1. Comparison of tissue penetration ability of 808- and 880-nm lasers.[a] Related to Scheme 1, and Figure 3 and 4.

	Remaining Power (%)	
Pork slide thickness (mm)	808-nm laser	880-nm laser
0.5	35.25 ± 1.1	57.75 ± 0.3
1.0	19.18 ± 0.9	35.47 ± 0.9
1.5	13.37 ± 0.5	22.88 ± 1.2

[a] We measured the percentage of the remaining power of a beam from 808- or 880-nm laser (0.8 W cm^{-2}) after it penetrated the pork slides with different thicknesses.

SUPPLEMENTAL FIGURES

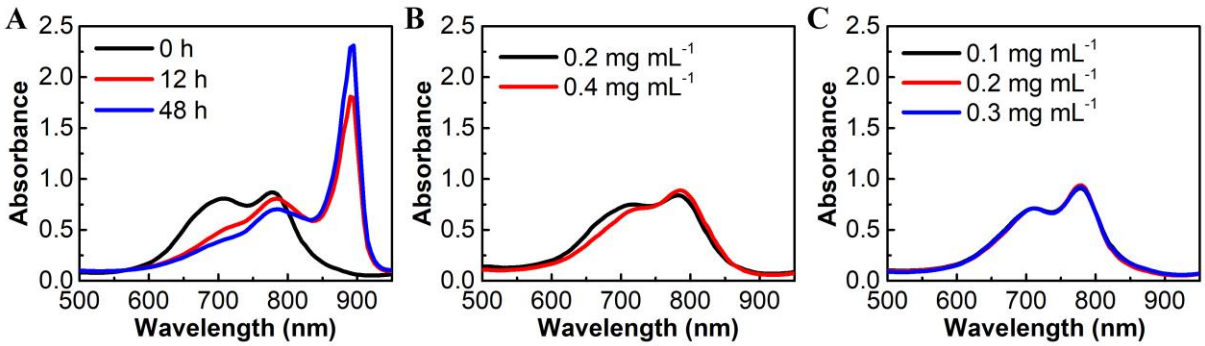

Figure S1. Monitoring ICG aggregation under different conditions via absorption spectrum. (A) In the presence of DSPE-PEG_{2k}-NH_2 (0.2 $mg \cdot mL^{-1}$) with room-temperature stirring in water. (B and C) Mixing with different concentrations of (B) DSPE-PEG_{2k} and (C) PEG_{2k}-NH_2 in water after 24 h of stirring at room temperature. In all the experiments, the concentration of ICG was 50.0 μg mL^{-1}. Related to Figure 1.

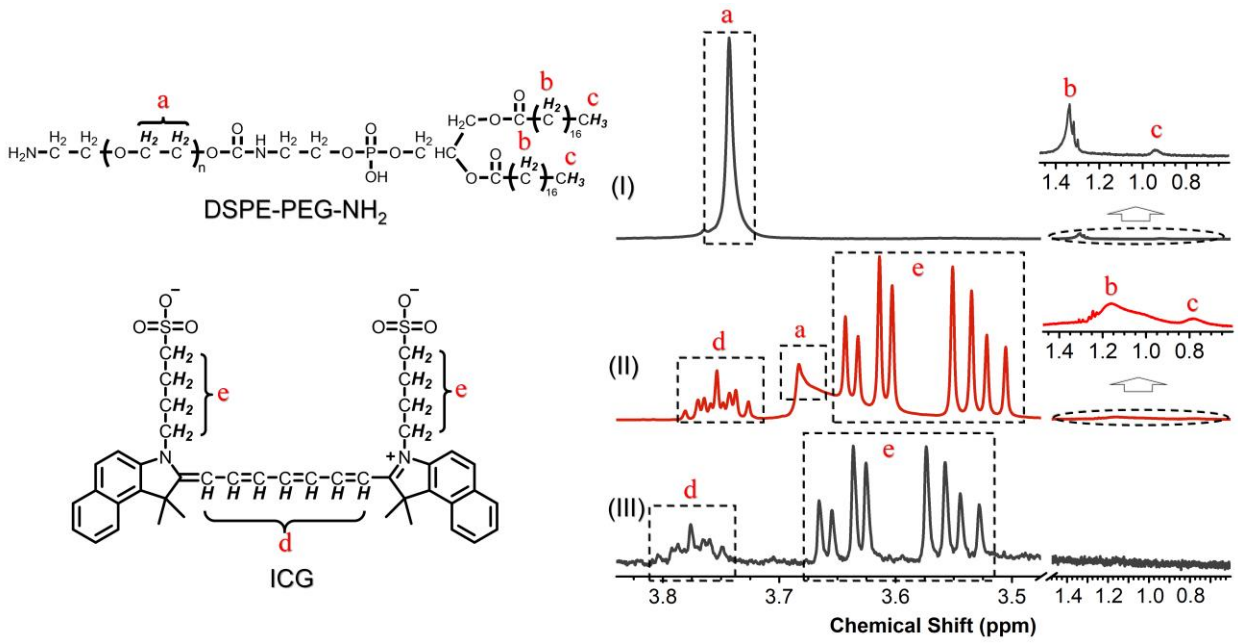

Figure S2. ^1H NMR spectra of (I) DSPE-PEG_{2k}-NH_2 micelle, (II) DSPE-PEG_{2k}-NH_2 micelle with ICG J-aggregate in encapsulation, and (III) naked ICG J-aggregate, as well as the assignment of the peaks. Related to Figure 1.

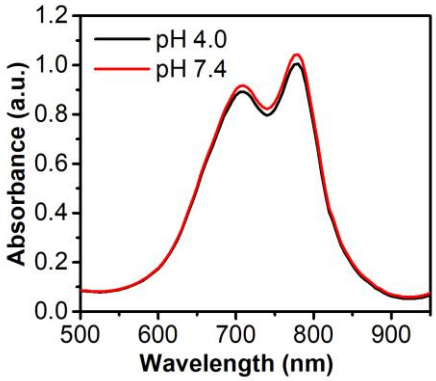

Figure S3. The absorption spectra of ICG (10.0 mg mL^{-1}, PBS buffers of pH 4.0 and 7.4) after a 24-h stirring at room temperature. The solutions were diluted with corresponding buffer before the tests. Related to Figure 1.

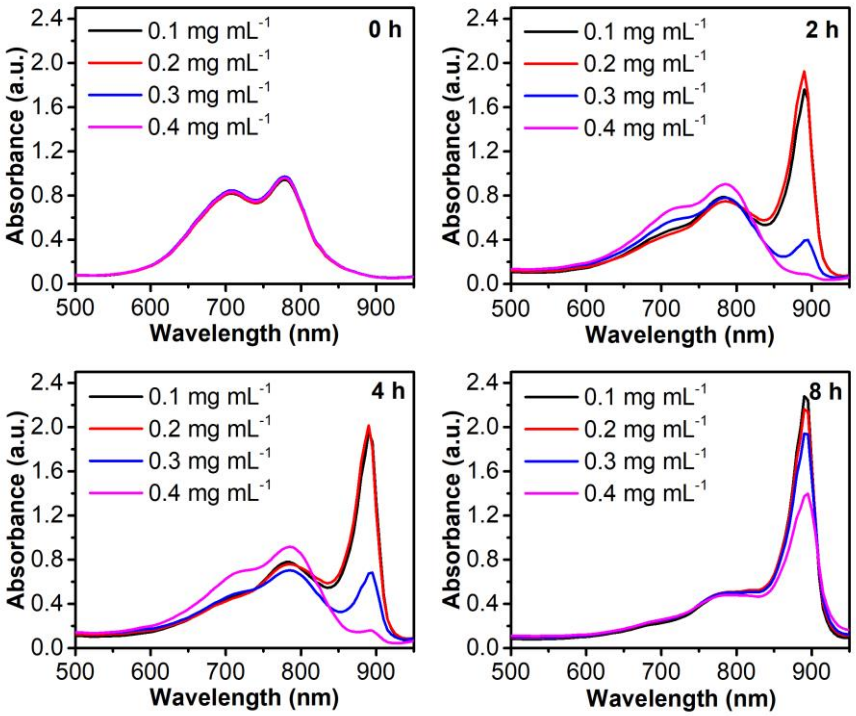

Figure S4. The absorption spectra of the aqueous mixtures between ICG (50.0 μg mL^{-1}) and different concentrations of DSPE-PEG_{2k}-NH_2. The mixtures were first heated at 80 °C for 15 min,

thereafter their absorption spectra were detected at different time points during the subsequent stirring process. Related to Figure 2.

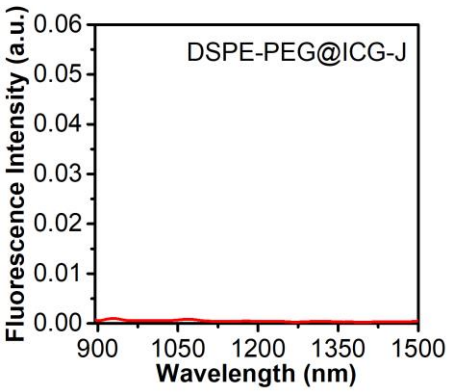

Figure S5. The fluorescence spectrum of DSPE-PEG@ICG-J, which was excited at wavelength of 880 nm. Related to Figure 2.

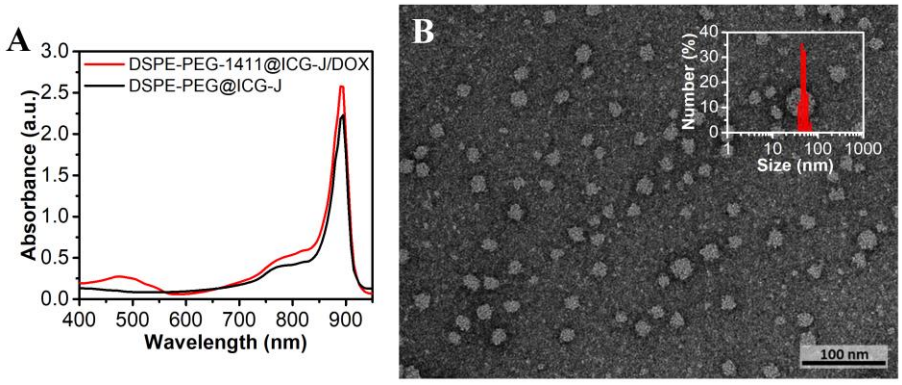

Figure S6. (A) The absorption spectrum of DSPE-PEG-1411@ICG-J/DOX (the red line), in which a typical peak at 480 nm was additionally observed as compared with the absorption of DSPE-PEG@ICG-J (the black line), indicating that DOX has been successfully loaded to the micelles.

(B) The TEM image and DLS characterization result (inset) of DSPE-PEG-1411@ICG-J/DOX. Related to Figure 3 and 4.

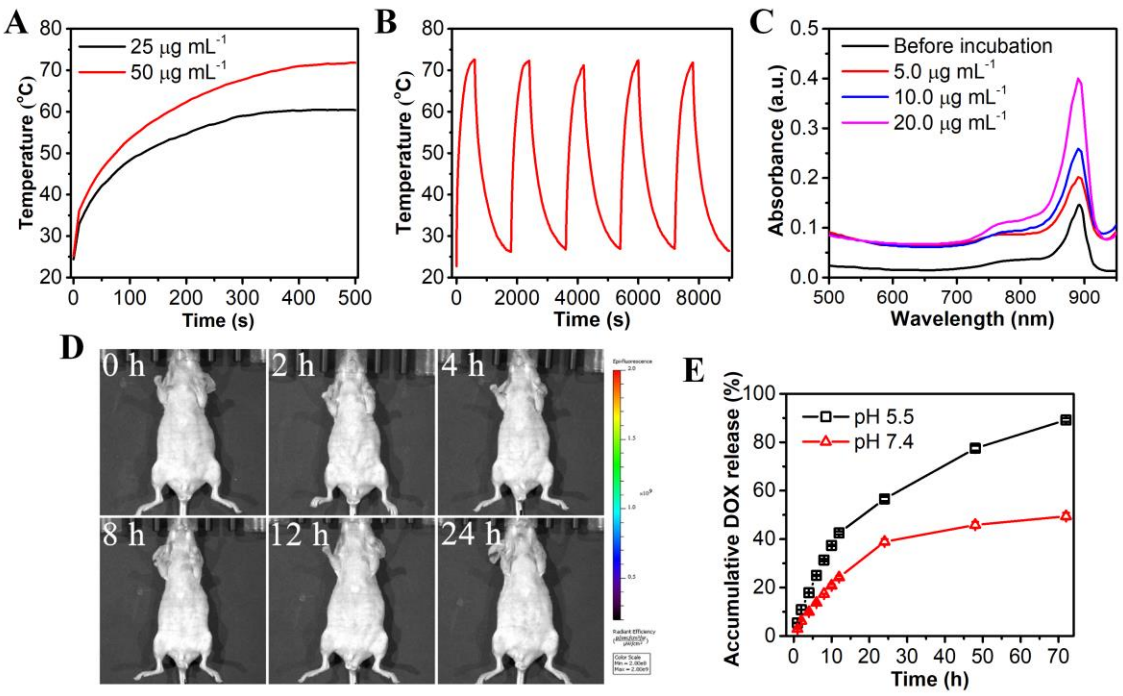

Figure S7. Detection of the photothermal conversion efficiency, the stability, and the drug release profiles of DSPE-PEG-1411@ICG-J/DOX. (A) The photothermal heating curves of DSPE-PEG-1411@ICG-J/DOX solution at different concentrations under 880-nm laser irradiation at a power density of 0.8 W cm^{-2} for 500 s. (B) Temperature change of DSPE-PEG-1411@ICG-J/DOX solution (ICG concentration equivalent to 50.0 μg mL^{-1}) recorded every 10 s during five circles of 10-min with irradiation (heating) and 20-min without irradiation (cooling) processes. (C) The absorption spectra of the suspensions of A549 cells incubated with DSPE-PEG-1411@ICG-J/DOX at different concentration for 4-h. (D) The fluorescence images obtained by the animal fluorescence imaging system at different time points after 150.0 μL of DSPE-PEG-1411@ICG-J/DOX solution (ICG concentration equvalent to 0.5 mg mL^{-1}) was intravenously injected to BALB/c nude mice. (E) *In vitro* DOX-release profiles of DSPE-PEG-1411@ICG-J/DOX in PBS

buffer (pH 7.4) and HAc-NaAc buffer (pH 5.5). Error bars indicate standard errors of triplicate tests. Related to Figure 3 and 4.

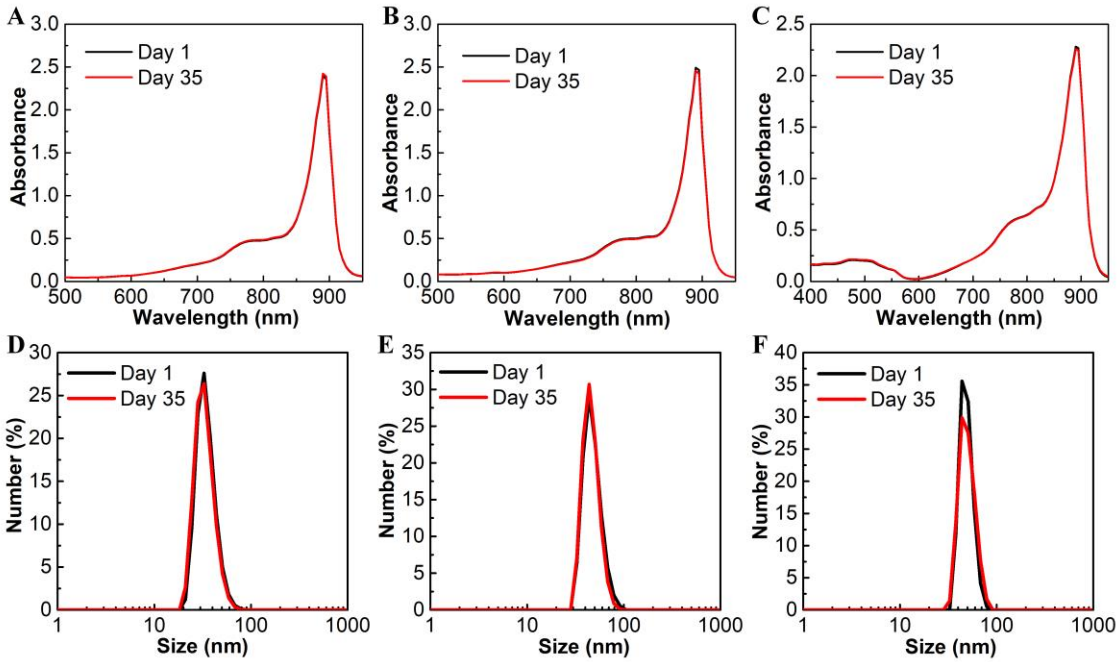

Figure S8. The absorption spectra and DLS analysis results of (A, D) DSPE-PEG@ICG-J, (B, E) DSPE-PEG-1411@ICG-J, and (C, F) DSPE-PEG-1411@ICG-J/DOX at the first day (Day 1) and last day (Day 35) of the long-term stability detection. Related to Figure 3 and 4.

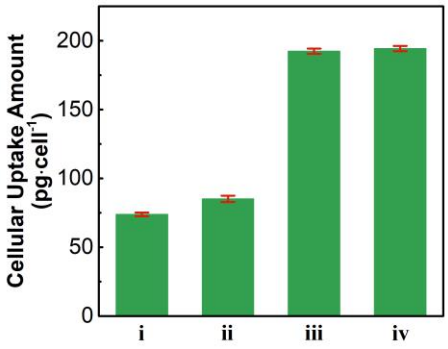

Figure S9. The cellular uptake results of i) ICG, ii) DSPE-PEG@ICG-J, iii) DSPE-PEG-1411@ICG-J, and iv) DSPE-PEG-1411@ICG-J/DOX in live A549 cells after 4-h incubation. For all the samples, ICG concentration equivalent to 25.0 μg·mL^{-1}. Data are presented as the average ± SD (n = 3). Related to Figure 4.

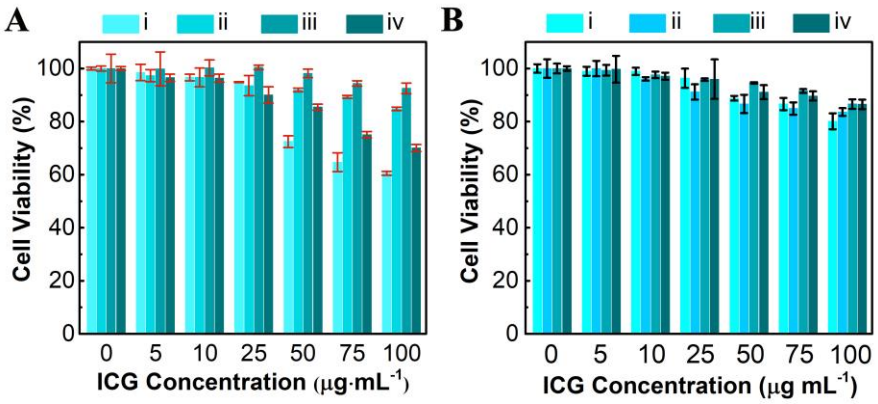

Figure S10. The dark cytotoxicity of i) ICG, ii) DSPE-PEG@ICG-J, iii) DSPE-PEG-1411@ICG-J, and iv) DSPE-PEG-1411@ICG-J/DOX to (A) A549 and (B) normal L02 cells determined by MTT assay. Error bars indicate standard errors of quintuple tests. Related to Figure 4.

The dark cytotoxicities of DSPE-PEG@ICG-J, DSPE-PEG-1411@ICG-J, and DSPE-PEG-1411@ICG-J/DOX were tested on A549 and normal human hepatic L02 cell lines by MTT assay to evaluate their biocompatibilities at the cellular level, where free ICG was used as a comparison. At concentrations larger than 50 μg·mL^{-1}, the free ICG started to show cytotoxicity, while the complex micelles loaded with equivalent amounts of ICG showed negligible cytotoxicity (Figure S9). The results demonstrated that the biocompatibility of ICG has been further improved through DSPE-PEG encapsulation. In addition, AS1411 conjugation did not bring any side effect to the

complex micelle. DSPE-PEG-1411@ICG-J/DOX did show some cytotoxicity at high concentrations, which should be caused by the intrinsic toxicity of DOX.

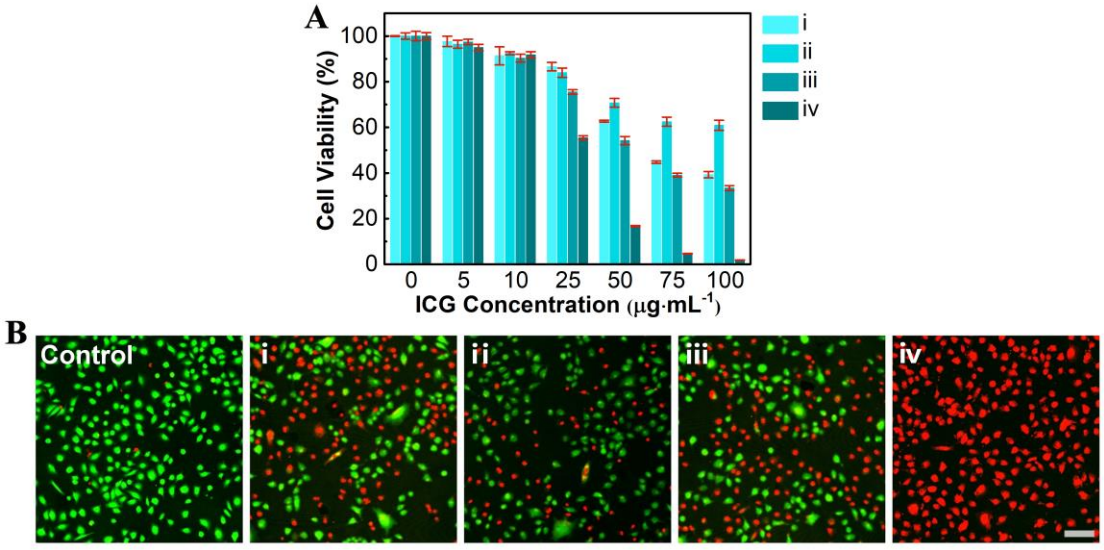

Figure S11. The *in vitro* anticancer therapy study result. Sample: i) ICG; ii) DSPE-PEG@ICG-J; iii) DSPE-PEG-1411@ICG-J; iv) DSPE-PEG-1411@ICG-J/DOX. (A) Viability of A549 cells following PTT with various samples for 10 min laser irradiation (0.8 W cm^{-2}, 808-nm laser for ICG, and 880-nm laser for the micelles); data are presented as the average ± SD (n = 5). (B) Fluorescence images of Calcein AM/PI stained A549 cells incubated with various samples (ICG concentration equivalent to 100 μg·mL^{-1}) after PTT. The scale bar is 100 μm. Related to Figure 4.

In the *in vitro* anticancer therapy study, in order to clarify the role of each component in the final complex micelle, DSPE-PEG@ICG-J, DSPE-PEG-1411@ICG-J, and DSPE-PEG-1411@ICG-J/DOX were systematically investigated to elucidate the PTT effect of ICG J-aggregates, the targeting effect of AS1411, and the chemotherapy effect of DOX. In detail, the samples (the amounts were normalized by ICG concentration) were incubated with A549 cells for

4 h, thoroughly washed by PBS, and then irradiated by laser at a power density of 0.8 $W \cdot cm^{-2}$ for 10 min; finally, the cell viability was evaluated by MTT assay after an additional 24-h culture. Notably, lasers at different wavelengths were selected to match the optimal absorptions of free ICG (808 nm) and ICG J-aggregate (880 nm). As shown in Figure S10A, from an ICG equivalent concentration of 50 $\mu g \cdot mL^{-1}$, free ICG and DSPE-PEG@ICG-J started to show visible cytotoxicity. The group of free ICG showed higher cytotoxicity compared with the group of DSPE-PEG@ICG-J, which mainly came from the intrinsic cytotoxicity of ICG at high concentrations according to the results of dark cytotoxicity test. On the other hand, after irradiation, the cytotoxicity of DSPE-PEG@ICG-J increased with respect to that under dark condition, which demonstrated the toxic PTT effect of ICG J-aggregate. After the integration of AS1411 aptamer, significantly intensified cytotoxicity was observed from DSPE-PEG-1411@ICG-J, indicating that a 2.6-fold improvement in cellular uptake by the presence of AS1411 greatly facilitated the PTT effect of the complex micelles. Finally, DSPE-PEG-1411@ICG-J/DOX which integrated with three functionalities could kill 99.2% cells at an ICG equivalent concentration of 100 $\mu g \cdot mL^{-1}$. This cell-killing rate was much better than those in the PTT dominant group (DSPE-PEG-1411@ICG-J with irradiation) and the chemotherapy dominant group (DSPE-PEG-1411@ICG-J/DOX without irradiation). Therefore, we concluded that the remarkably enhanced anticancer efficacy of DSPE-PEG-1411@ICG-J/DOX under laser irradiation derived from the synergistic interaction between chemotherapy and PTT; the similar synergistic effect has been observed in many other related studies and considered as an efficient anticancer strategy (Yan et al., 2018; Zhang et al., 2018; Wang et al., 2018; Xu et al., 2019). To further visualize the cancer cell killing effect contributed from PTT, targeting, and chemotherapy, the above cells treated with free ICG and micelles (ICG equivalent concentration at 100 $\mu g \cdot mL^{-1}$) were stained with calcein acetoxymethyl ester (Calcein-

AM) and propidium iodide (PI) to identify live and dead/late apoptotic cells (Figure S10B). The result was inconsistent with the MTT assay result, indicating the remarkable anticancer efficacy of DSPE-PEG-1411@ICG-J/DOX through synergistic enhancement of its respective components.

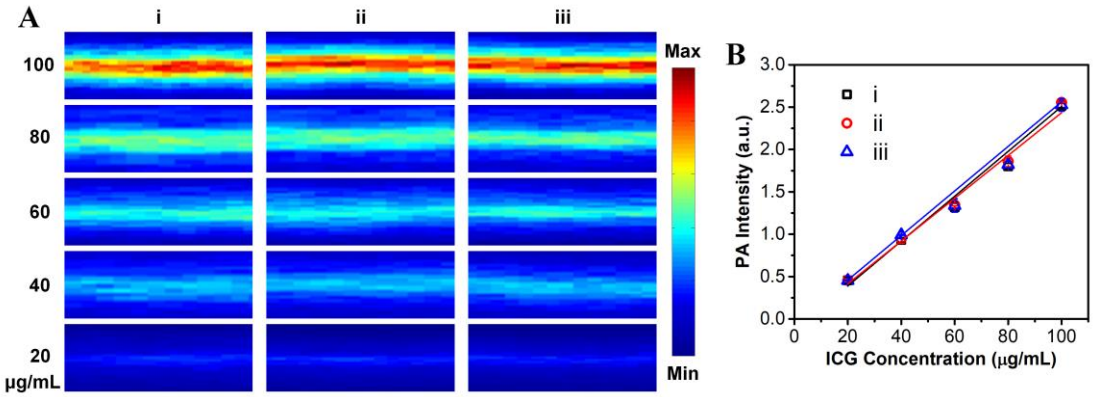

Figure S12. *In vitro* determination of the photoacoustic properties of i) DSPE-PEG@ICG-J, ii) DSPE-PEG-1411@ICG-J, and iii) DSPE-PEG-1411@ICG-J/DOX. (A) The PA images of the micelles upon excitation at 880 nm (pulsed laser) at different ICG equivalent concentrations. (B) PA intensities of the micelles at 880 nm as a function of ICG equivalent concentrations. Related to Figure 3.

Since the photoacoustic response of the three kinds of complex micelles all comes from the ICG J aggregates encapsulated in them, they displayed consistent photoacoustic signals at the same ICG equivalent concentrations.

The photoacoustic signal intensities of the complex micelles are linearly related to their ICG equivalent concentrations.

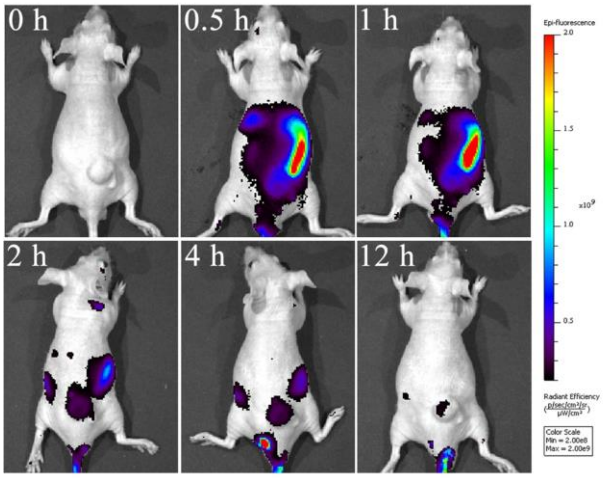

Figure S13. The fluorescence-indicated metabolism of ICG in mouse. The fluorescence images obtained by animal fluorescence imaging system at different time points after 150.0 μL of ICG solution (0.5 mg mL^{-1}) was intravenously injected to the BALB/c nude mice. Related to Figure 3.

The result demonstrated that ICG would reach the maximum accumulation at the tumor-site about 1 h after the intravenous injection.

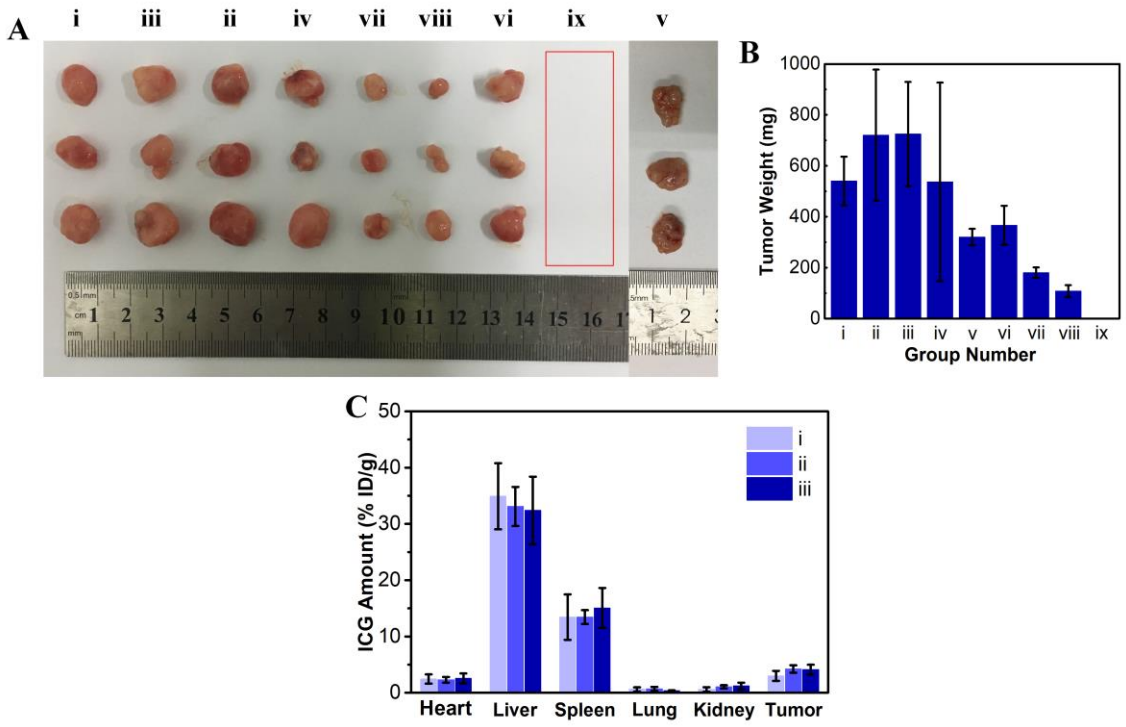

Figure S14. The (A) pictures and (B) weights of the tumors collected 24 days after the treatments: i) Control; ii) DOX; iii) PBS + 880-nm laser; iv) ICG + 808-nm laser; v) Doxil; vi) DSPE-PEG-1411@ICG-J/DOX; vii) DSPE-PEG@ICG-J + 880-nm laser; viii) DSPE-PEG-1411@ICG-J + 880-nm laser; ix) DSPE-PEG-1411@ICG-J/DOX + 880-nm laser. The power density of both 808-nm and 880-nm lasers is 0.8 W cm^{-2}. (C) *Ex vivo* bio-distributions of i) DSPE-PEG@ICG-J, ii) DSPE-PEG-1411@ICG-J, and iii) DSPE-PEG-1411@ICG-J/DOX in the main organs and tumor tissues of mice at 12 h post intravenous administration (n = 3). In the experiment, intravenous injection valume of the samples is 150.0 μL, for ICG and the micelles, ICG concentration equivalent to 0.5 mg·mL^{-1}; for DOX and Doxil, DOX concentration equivalent to 0.3 mg·mL^{-1}. Related to Figure 4.

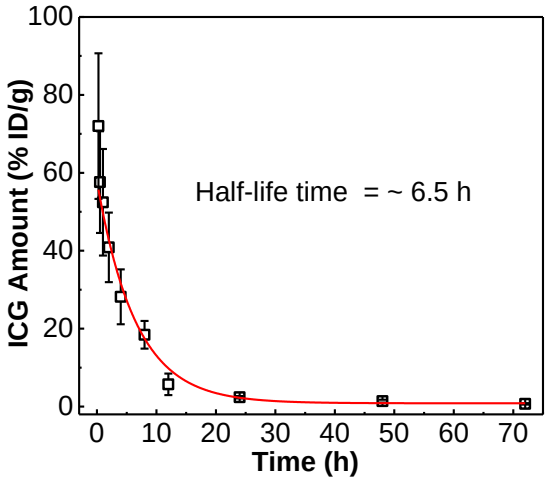

Figure S15. Blood circulation analysis of SD rats intravenously injected with DSPE-PEG-1411@ICG-J/DOX (at ICG equivalent dose of 4 mg kg^{-1}). Related to Figure 4.

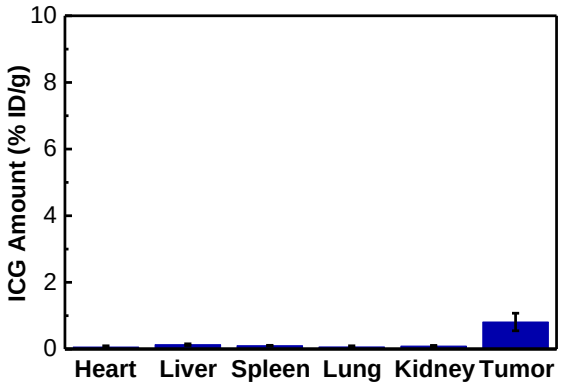

Figure S16. *Ex vivo* bio-distribution of DSPE-PEG-1411@ICG-J/DOX in the main organs and tumor tissues of mice at 7 days post intravenous administration (n = 3). 150 μL of DSPE-PEG-1411@ICG-J/DOX was injected at ICG equivalent concentration of 0.5 mg·mL^{-1}. Related to Figure 4.

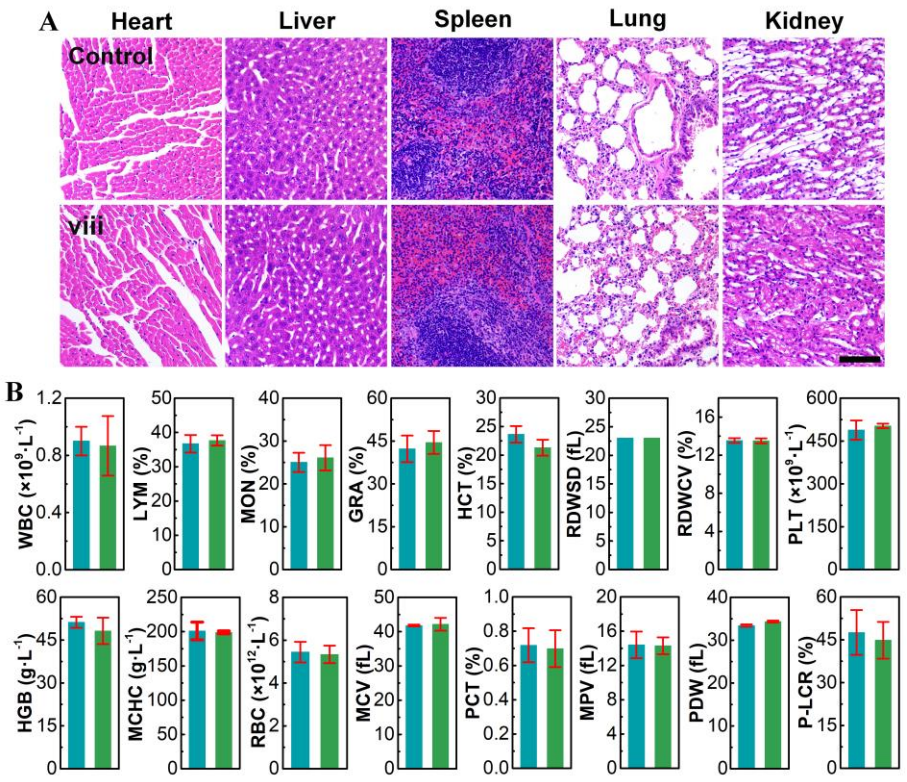

Figure S17. Histology and blood tests of the healed mice in the *in vivo* anticancer therapy study. (A) Histological H&E staining for different organs collected from mice in group ix, and the organs in control group were collected from health mice. The scale bar is 100 μm. (B) Blood tests for healthy mice (blue bars) and the mice in group ix (green bars), data are presented as the average ± SD (n = 3). Related to Figure 4.

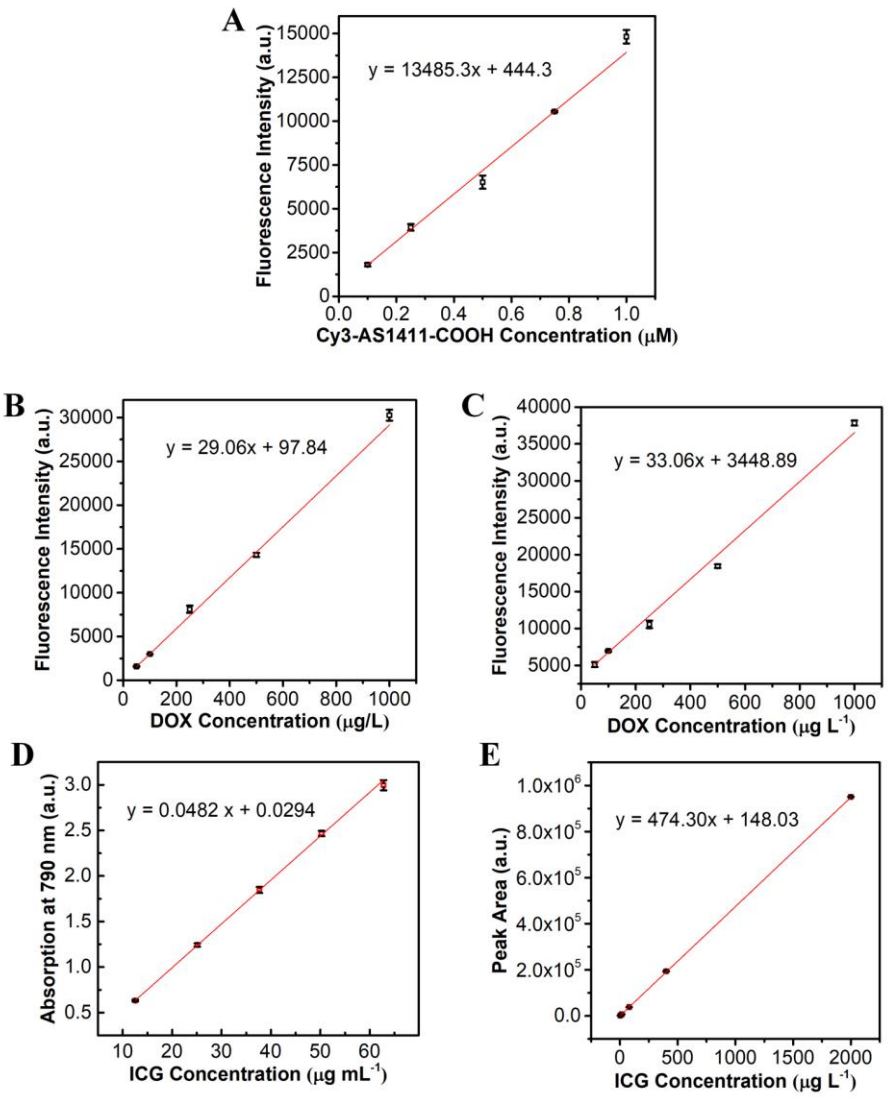

Figure S18. The calibration curves. (A) The fluorescence calibration curve of Cy3-AS1411-COOH, the excitation wavelength was 500 nm, and the emission was measured at wavelength of 565 nm. The fluorescence calibration curve of DOX in (B) PBS (pH 7.4) and (C) HAc-NaAc buffer (pH 5.5), the excitation wavelength was 488 nm, and the emission was measured at the wavelength of 595 nm. (D) The absorption calibration curve of free ICG for the cellular uptake study. (E) The absorption calibration curve of ICG for the bio-distribution study. Related to Figure 3 and 4.

Supplemental References

Yan, G. W., Li, A. H., Zhang, A. T., Sun, Y., and Liu, J. Q. (2018). Polymer-based nanocarriers for co-delivery and combination of diverse therapies against cancers. Nanomaterials *8*, 85.

Zhang, A., Li, A., Zhao, W., and Liu, J. (2018). Recent advances in functional polymer decorated two-dimensional transition-metal dichalcogenides nanomaterials for chemo-photothermal therapy. Chem.-Eur. J. *24*, 4215-4227.

Wang, J., Dong, Y., Li, Y., Li, W., Cheng, K., Qian, Y., Xu, G., Zhang, X., Hu, L., Chen, P., et al. (2018). Designer exosomes for active targeted chemo-photothermal synergistic tumor therapy. Adv. Funct. Mater. *28*, 1707360.

Xu, Y., Chen, J., Tong, L., Su, P., Liu, Y., Gu, B., Bao, B., and Wang, L. (2019). pH/NIR-responsive semiconducting polymer nanoparticles for highly effective photoacoustic image guided chemo-photothermal synergistic therapy. J. Control. Release *293*, 94-103.